

Article

Numerical Simulation of a Thermal Management System Using Composite Flame-Retardant Resin and Its Effect on Battery Life Span

Florin Mariasiu ^{*}, Ioan Szabo  and Thomas I. C. Buidin

Technical University of Cluj Napoca, EMARC Research Centre, Blvd. Muncii 103-105, 400114 Cluj-Napoca, Romania; ioan.szabo@auto.utcluj.ro (I.S.); thomas.buidin@auto.utcluj.ro (T.I.C.B.)

* Correspondence: florin.mariasiu@auto.utcluj.ro

Abstract: One of the obstacles to the adoption of electric vehicles as a future pollution-free transport solution is that the energy sources (batteries) have not yet become sustainable through a long-life span under the specific operating conditions. The problem that arises is that high temperatures inside the batteries represent a safety risk and have negative effects on the battery life span, which imposes the use of thermal management systems. The present article aims to analyze, by numerical methods, the effect of the use of a fireproof composite resin on the efficiency of the thermal management system, specifically on the degree of battery sustainability (measured by the effect on the life span). Five constructive variants are proposed and thermally analyzed. Based on the measured temperatures, the intensity of the chemical reactions that occur in a 18650-type Li-ion cell was calculated, and conclusions related to the impact on the life span were drawn. It has been found that the use of a fireproof composite resin leads to an increased heat transmission towards the outer environment and an increase in the life span by 22.2% compared to that noted for conventional air cooling. The results also recommend the use of heat exchangers associated with flame retardant resins, which leads to a 20.6% improvement in the heat transfer capacity of the battery's thermal management system. When comparing the solutions in which the flame-retardant resin is used, the results show that adding 3 wt.% of nanomaterial leads to a significant life span increase of 11.7% when compared to the results for the resin-only case.

Keywords: battery; thermal management; flame retardant resin; life span; intensity of chemical reactions



Citation: Mariasiu, F.; Szabo, I.; Buidin, T.I.C. Numerical Simulation of a Thermal Management System Using Composite Flame-Retardant Resin and Its Effect on Battery Life Span. *Sustainability* **2024**, *16*, 3702. <https://doi.org/10.3390/su16093702>

Academic Editors: Damir Jakus and Josip Vasilj

Received: 12 March 2024

Revised: 22 April 2024

Accepted: 24 April 2024

Published: 28 April 2024



Copyright: © 2024 by the authors. Licensee MDPI, Basel, Switzerland. This article is an open access article distributed under the terms and conditions of the Creative Commons Attribution (CC BY) license (<https://creativecommons.org/licenses/by/4.0/>).

1. Introduction

One of the fully accepted solutions related to the reduction of environmental pollution is the use of large-scale sustainable transportation. The electric vehicle is a certainty in this sense, and in recent years, numerous efforts have been to achieve its massive introduction into the car market [1]. However, the use of electric vehicles raises questions related to their sustainability, and it is generally accepted that the manufacturing method of both electric vehicles and their components must be a sustainable process [2]. It should be noted that the production process of batteries involves the extraction and processing of numerous metals and minerals (lithium, cobalt, nickel, manganese, and graphite) with polluting potential [3,4]. The mining activities associated with the extraction of these metals and minerals cause damage to the environment through water pollution, soil erosion, habitat loss, energy consumption, and the industrial emission of greenhouse gases [5].

The disposal and recycling of electric vehicle batteries is another important aspect to consider from a sustainability point of view. Batteries have a limited lifespan and after the loss of a significant portion of their capacity, they can be repurposed (storage of solar and/or wind energy) or recycled to recover valuable materials, avoiding the accumulation of hazardous waste occurring through storage and/or destruction [6–8].

One way to increase the sustainability of electric vehicles is through increasing the energy efficiency, life span, and operational safety of the battery, efforts which directly depend on several factors, such as electrochemistry, charging mode, environmental conditions, and driving style.

Extreme temperatures, including those that are either too low or too high, reduce battery performance because they affect the rate of chemical reactions inside the cells [9,10]. At low temperatures, the internal resistance of the batteries increases, which means that they supply less power to the electric motor [11]. Additionally, batteries can become more fragile and more susceptible to cracking or short-circuiting. At high temperatures, the batteries discharge faster, which reduces the range of the electric vehicle. Moreover, batteries can emit toxic or flammable gases, which can be dangerous to human health or cause fire incidents. Therefore, most electric vehicle batteries include thermal management systems that maintain the optimal operating temperature, usually between 20 and 50 °C [12].

Battery life refers to the number of charge and discharge cycles the battery can perform before losing a significant portion of its capacity. Extreme temperatures accelerate the degradation of batteries because they cause the deterioration of the cells' internal structure, the formation of deposits on the electrodes, or the loss of electrolyte [13,14]. At high temperatures, batteries can suffer from a phenomenon called "thermal runaway", which consists of an uncontrolled increase in temperature and internal pressure, leading to explosion or fire risks [15]. Therefore, it is important to take preventative measures in two specific areas: the avoidance of battery overheating (especially during fast charging) and maintaining an optimal battery state of charge (SoC) level, preferably between 20 and 80% [16].

In order to fulfill the above requirements regarding safety and corresponding exploitation, different battery thermal management systems (BTMS) have been researched and developed. Most BTMSs are designed to cool and remove heat from the battery pack (to maintain an optimal temperature) using active, passive, and hybrid methods, each of which has advantages and disadvantages, depending on the field of application [17]. Active management methods require power consumption for their operation and are related to air cooling, liquid cooling, and thermoelectric cooling [18]. Passive systems rely on natural thermal phenomena, such as convection and radiation, using heat sinks, phase-change materials, and heat pipes, while hybrid methods combine active and passive techniques [19]. The advantages and disadvantages of using different BTMSs are presented in many scientific works, and a summary of the conclusions related to this aspect can be found in Tables 1 and 2.

Table 1. Analysis of passive BTMSs.

Passive BTMS Type	Advantages	Disadvantages
Phase change materials	<ul style="list-style-type: none"> Reduced costs Long life span Uniform temperature distribution High latent heat Stability over a wide range of temperatures 	<ul style="list-style-type: none"> Low thermal conductivity Possible sealing problems Limited heat recovery capacity if the stored heat is not efficiently dissipated Considerable mass
Heat pipes	<ul style="list-style-type: none"> Very high thermal conductivity High efficiency Compactness No required maintenance Long life span 	<ul style="list-style-type: none"> High costs Condenser cooling by natural convection only is insufficient

Table 2. Analysis of active BTMSs.

Active BTMS Type	Advantages	Disadvantages
Forced air convection	<ul style="list-style-type: none"> Easy applicability Direct contact between coolant and accumulators Reduced mass Reduced costs Simple construction Easy maintenance 	<ul style="list-style-type: none"> Low specific heat Large volume required Difficult to achieve a uniform distribution of air flow Uneven temperature distribution Low efficiency
With liquid by direct contact	<ul style="list-style-type: none"> High thermal conductivity Superior heat transfer coefficient (compared to air cooling and indirect liquid cooling) 	<ul style="list-style-type: none"> High mass Possible sealing problems Risk of short circuit
With liquid through indirect contact	<ul style="list-style-type: none"> Easy to implement (compared to direct contact cooling) Compactness Good heat transfer capacity 	<ul style="list-style-type: none"> Poorer cooling performance (compared to direct contact cooling) Large pressure drops Thermal inhomogeneity in the case of long flow channels
With refrigerant	<ul style="list-style-type: none"> High performance Relatively easy integration into vehicles Possibility of cooling below ambient temperature Possibility of heating 	<ul style="list-style-type: none"> Risk of refrigerant overheating due to heat load from two sources (cabin comfort and battery) Risk of thermal non-uniformity in case of intense cooling
Thermoelectric modules	<ul style="list-style-type: none"> Static device No production of noise or vibration Long life span Minimal maintenance costs Possibility of cooling below ambient temperature Possibility of battery heating Temperature control with high precision Compactness 	<ul style="list-style-type: none"> Low efficiency High power consumption High costs Proximity of the cooled side to the hot side of the module

Most of the research carried out on the effect of integrating resins into the system focused on evaluating the possibilities for heat transfer from the batteries to the external environment. Extensive research has been conducted by adding aluminum nitride, copper powder and carbon fiber (in different ratios) as thermally conductive fillers to a silicon-based matrix. The obtained composite material was then used to cover prismatic batteries, which has led to an improved heat dissipation [20,21]. A modified silicone-based resin, resulting from adding 1 wt.% spherical boron nitrides, was used as a thermal interface on the surface of the liquid cooling plate of a battery module [22]. It was found that the maximum temperature of the battery module could be maintained within the operational limit of 42 °C, as well as that the temperature difference could be controlled within 5 °C by BTMS. Also, an expanded graphite/paraffin/silicone rubber composite phase-change material was developed as a thermal interface, with a high thermal conductivity ($0.56 \text{ W}\cdot\text{m}^{-1}\cdot\text{K}^{-1}$) [23].

A less researched method involves combining thermal management systems with fire-resistant materials as a safety measure against the risk of battery fire due to road accidents. In this context, there is a need for the research and identification of BTMSs that offer relevant solutions to increase the sustainability of electric vehicle batteries, through measures that extend operational life and reduce the operation-associated risks [24].

This article presents a comparative analysis of the effect of using a composite material that meets the UL94 V-0 flame-retardancy standard on a Li-ion battery module's lifespan, by simulation. This is due to the need to analyze *a priori* the effects of using a flame retardant resin on the heat transfer process, later determining whether it is necessary to continue the experimental (applied) research. The major advantage of using computer simulations is

that the associated costs are very low, and the results are obtained in a very short time. The aim of research methodology is to consider the number of chemical reactions (a function of temperature variation) and specifically, the intensity of degradation processes that occur in the cells.

The structure of the article is as follows: in Section 1, the concept of battery sustainability is analyzed in regards to the influence of operating temperatures, and a general classification of BTMSs is presented; Section 2 presents the methods, methodology, and cases considered for numerical analysis; Section 3 presents the results obtained through the simulation of the considered cases, together with the analysis and discussions regarding the effect of each proposed constructive solution on the cells' lifetime. The conclusions and the identification of new development directions can be found in Section 4.

2. Materials and Methods

2.1. Research Methodology

The creation and simulation of the battery models was achieved with CAD (Solid Works2024, Flow Simulation SP Version 1.0 Build: 6234) design software, the configuration of the 18,650 Li-ion cells that form the battery module subjected to the simulation being of the 4S4P (four series four parallel) type. The entire five-case simulation was run on a system with an Intel(R) Xeon(R) Gold 6134 CPU @ 3.20GHz, 130,693 MB of RAM, and Windows 10 (Version 10.0.19045), analyzing both laminar and turbulent fluid flow with heat transfer and forced convection. For Case #1, the mesh created for the battery module included 1,223,557 discretized cells. The mesh utilized a total of 234,274 fluid cells to accurately model fluid dynamics, 989,283 solid cells to represent the battery structure, and 156,813 partial cells. The meshing process reached convergence after 300 iterations, lasting a total of 1867 s. In Case #2, the same technique was used to create a discretized mesh for the battery module, which resulted in a total of 1,375,409 cells, including 119,452 fluid cells to represent fluid flow, 1,255,957 solid cells to depict the battery structure, and 66,018 partial cells. Mesh convergence was reached following 300 iterations, requiring a computational time of 1281 s. Significantly, there were no cells removed during the trimming procedure. Case #3 and Case #4 exhibited a meshing approach consistent with that of Case #2. Case #5 adopted a refined mesh strategy for the battery module, resulting in a total of 1,595,780 cells. This mesh comprised 190,554 fluid cells to capture intricate fluid behavior, 1,405,226 solid cells for detailed representation of the battery structure, and 106,466 partial cells. Notably, no cells were removed during the trimming process, indicating a well-defined mesh.

To validate the numerical model, the experimental data with the corresponding 10W average heat generation rate, obtained in our previous experiments, were used [25,26], which were compared to the data obtained by running the numerical model, in the case of the use of fire-retardant composite resin. The comparative results, together with the errors obtained for the considered battery discharge process, are presented in Figure 1. It can be stated that due to the heat absorption capacity of the surrounding material, the errors induced by the variation in the heat generation rate as a function of the depth of discharge (DoD) are mitigated, with an average temperature error of 1.5% and a maximum error of 1.9%. The final temperature values (60.8 °C during the experiment and 60.3 °C from the simulation) correspond, the error being of 0.9%, results that validate the numerical simulation approach proposed in this paper.

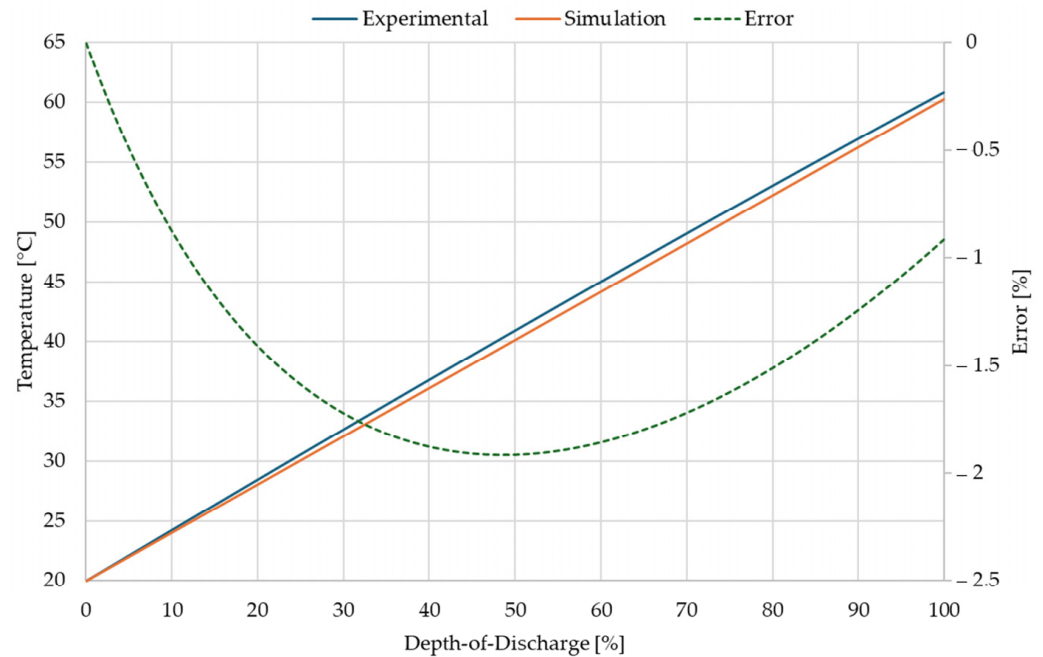


Figure 1. Measured and simulated temperature evolution and errors for a cell inside a battery module surrounded by fire-retardant composite material.

These analysis cases were thus chosen to compare, first of all, the influence of the main thermal characteristics of the used heat transfer medium material. Furthermore, the choice of materials also allowed for the analysis of their influence on the battery lifetime, by analyzing the intensity of the electrochemical reactions. In order to study the effect of using a flame-retardant composite material on the thermal transfer process of the heat generated by a Li-ion battery, a basic air-cooling thermal management system (Figure 2a) was used as a reference. Two additional models were developed, one using a fire-retardant composite resin component (Figure 2b,c), and one model with an aluminum block (Figure 2d). In addition, a complex model was developed that also incorporates a heat exchanger with aluminum fins, attached to the volume of the composite flame-retardant resin (Figure 2e and construction details are shown in Figure 3). The modeling and simulation methodology used for the considered models is presented in Figure 4.

The cases chosen for the analysis of the thermal transfer process were considered according to the thermal transfer environment of the heat generated by the cells to the outside environment, and these were labeled as follows:

1. Case #1—Air cooling (Figure 2a);
2. Case #2—Air cooling and the use of flame-retardant resin as a heat transfer medium (Figure 2b);
3. Case #3—Air cooling and the use of flame-retardant composite resin with nanomaterial fillers as a heat transfer medium (Figure 2c);
4. Case #4—Air cooling and the use of an aluminum block (Figure 2d);
5. Case #5—Air cooling and the use of flame-retardant composite resin with nanomaterial fillers and an aluminum heat exchanger as the heat transfer medium (Figures 2e and 3).

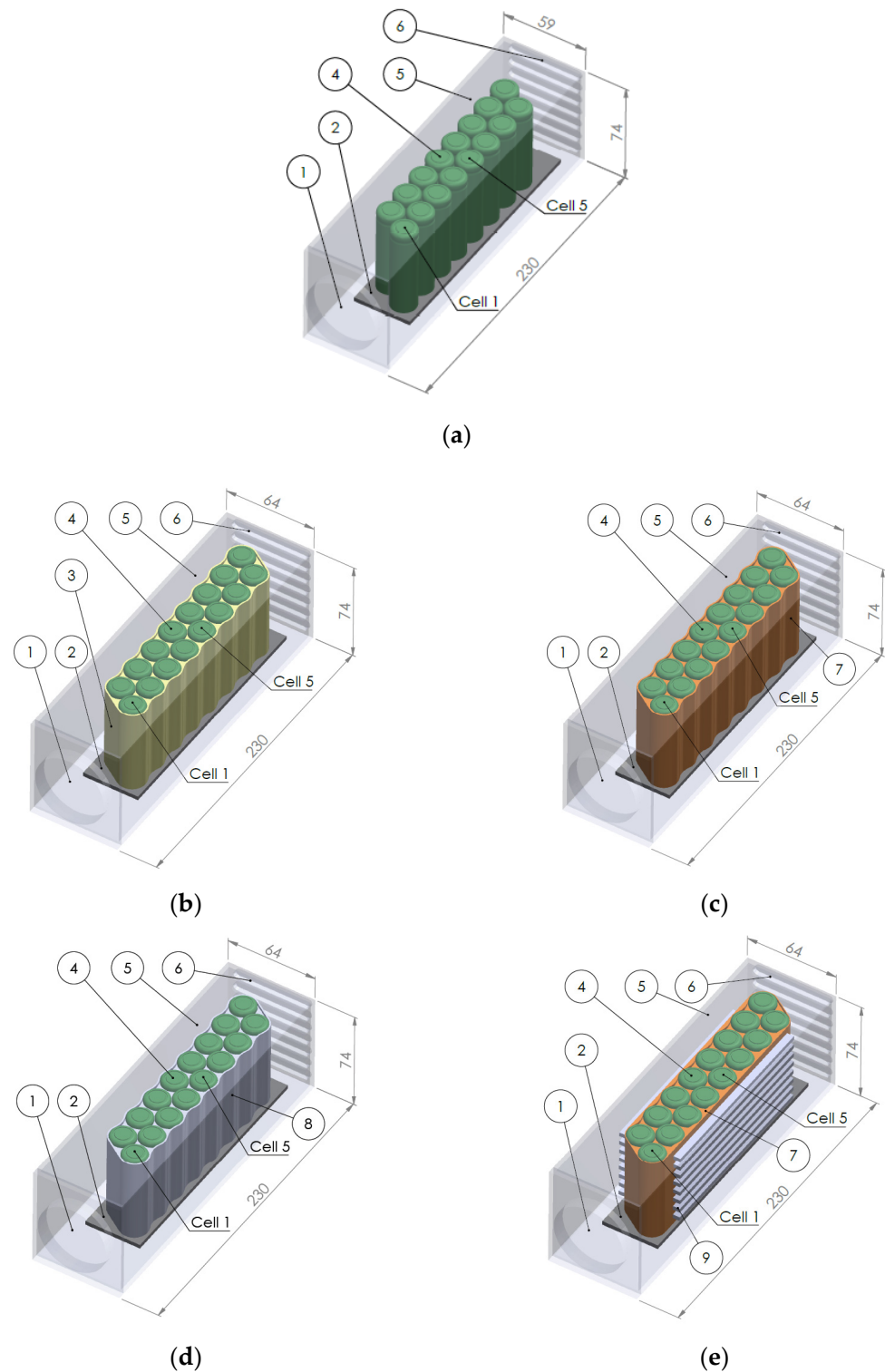


Figure 2. Considered models of the battery module in 4S4P organization: (a) air cooling; (b) air cooling and use of flame retardant resin; (c) air cooling and use of flame retardant composite resin with nanomaterials; (d) air cooling and aluminum block; (e) air cooling, use of flame retardant composite resin with nanomaterials, and aluminum side fins; 1—fan; 2—cell fixation support; 3—resin; 4—cell type 18650; 5—battery module housing; 6—air exhaust slots; 7—composite resin with nanomaterial (3 wt% boron nitride); 8—aluminum block; 9—aluminum fins.

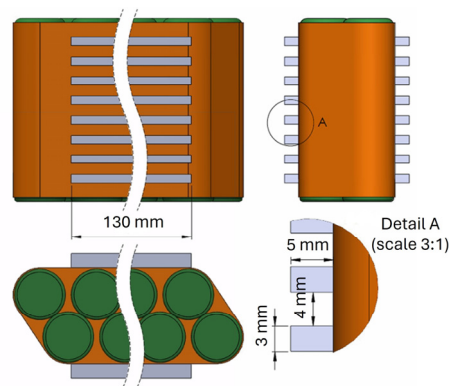


Figure 3. Construction details of the heat exchanger with aluminum fins for Case #5.

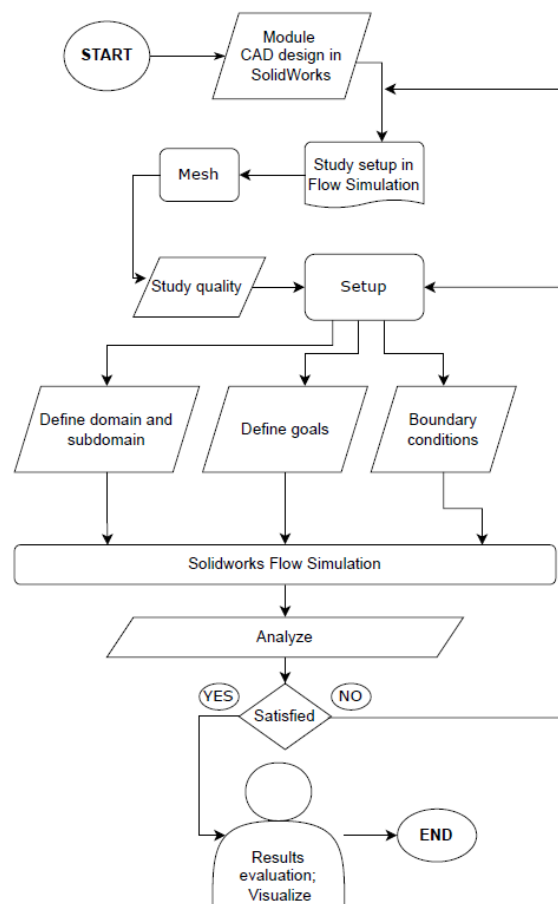


Figure 4. Modeling and simulation methodology used.

2.2. Defining Requirements

The simulation conditions were considered extreme, being carried out for 300 s for a heat generation rate of 160 W (10 W/cell), the generation rate corresponding to a battery discharge rate of 12 C. The cooling agent is air (with an initial temperature of 10 °C) at a flow rate of 150 m³/h (for a speed of 3000 min⁻¹). The measured temperatures were considered as those for cell #1 and cell #5. The characteristics and thermal parameters of the materials used in the construction of the battery model are presented in Table 3. Determining the thermal parameters required disc-shaped samples with a 10 mm diameter of two thickness values, 0.3 and 5 mm. The method used for these determinations is photopyroelectric calorimetry [27]. The working principle of photopyroelectric (PPE) is the optical irradiation of the sample, which partially transforms the radiation into heat.

The temperature modification of the sample is detected by a pyroelectric sensor, in direct thermal contact with the sample.

Table 3. Physical and thermal properties of battery components and BTMS.

Material	Density kg/m ³	Specific Heat J/(kgK)	Thermal Conductivity W/(mK)
Resin	1120	1400	0.20
Composite resin ²	2220	960	0.74
Battery cells	2725	960	3.35
Aluminum	2689	900 ¹	237

¹ @100 °C; ² according to Ref. [25].

The chosen basic matrix is an epoxy resin type ER2220 (producer Electrolube), being composed of two parts (resin + hardener/catalyst). This material has relatively high thermal conductivity (compared to other epoxy or silicone resins), good flow characteristics, and flame retardant behavior, according to the UL94 V-0 standard. The higher thermal conductivity value is obtained due to the presence of some fillers in the composition, namely zinc oxide and aluminum hydroxide, added by the manufacturer to the resin (the mass proportion of additive materials is 42% of the total). The technical data and the main properties of the resin before and after polymerization are presented in Tables 4 and 5. The fireproof composite resin has a 3 wt% ratio of added nanomaterials in its composition and the constant thickness of 1 mm around the battery module. The additive material chosen for conducting experimental research activities is hexagonal nano boron nitride, from the manufacturer PlasmaChem GmbH, Mainz, Germany, and the main technical data for the product is presented in Table 6.

Table 4. Main properties and parameters of liquid resin.

Parameter	Resin	Hardener
Color	Gray	Black
Density [g/mL]	2.38	0.3
Viscosity [mPa s @ 23 °C]	55000	25
Liquid mixture		
Viscosity [mPa s @ 23 °C]	1500	
Mass ratio	20.81:1	
Volumetric ratio	8.15:1	
Exploitable life span (@ 20 °C)	120 min	
	24 h @ 23 °C	
	4 h @ 60 °C	
Cure time	1 h @ 100 °C	
Reaction temperature	<35 °C	
Shrinkage	<1%	

Table 5. Main properties and parameters of solid resin after curing.

Parameter	Solid Resin
Color	Gray
Density [g/mL]	2.22
Operating temperatures [°C]	−40...130
Volume resistivity [ohm-cm]	10 ¹⁵
Dielectric strength [kV/mm]	10
Tensile strength [MPa]	60
Compressive strength [MPa]	120
Expansion coefficient [ppm/°C]	30

Table 6. Technical data of nano boron nitride.

Parameter	Value
Color and aspect	White powder
Average particle size	500 ± 100 nm
Full range of sizes	100–1000 nm
Specific surface area	23 ± 3 m ² /g
Purity	>98.5%
Nitrogen content	>55%
Density	approx. 2.25 g/cm ³

For Case #5, the construction of the heat exchanger was achieved by placing 16 lateral aluminum fins at the border of the resin structure, with the following geometric dimensions: length 130 mm, width 5 mm, and thickness 3 mm. The distance between the fins is 4 mm, the contact surface of the fins with the resin is 6240 mm², and the contact surface with the air is 27,520 mm².

3. Results and Discussion

3.1. Simulation Results

The results obtained after the simulation are presented in the following section, with an emphasis on the presentation of temperature variations for cells #1 and #5 of the battery module, which exhibit the largest temperature differences between each other, according to the battery module. Cell #1 is at the front and is the first cell to come in contact with the cooling air, showcasing the lowest temperature, and cell #5 is in the middle of the module and generally expresses the highest temperature. The values of temperature variation within the considered thermal process were further employed in the battery degradation calculation.

The application of the Arrhenius equation to calculate the temperature's influence on cell longevity requires a fundamental understanding of the impact that temperature changes have on the cells' performance and durability. In Figure 5 is presented the general configuration of battery module. The results of simulations, in terms of air and solid temperatures, are presented for each considered simulation case in Figures 6, 8, 10, 12 and 14. Figures 7, 9, 11, 13 and 15 illustrate the temperature variations that were obtained as a result of the simulations for each of the cases.

Case #1—Air Cooling

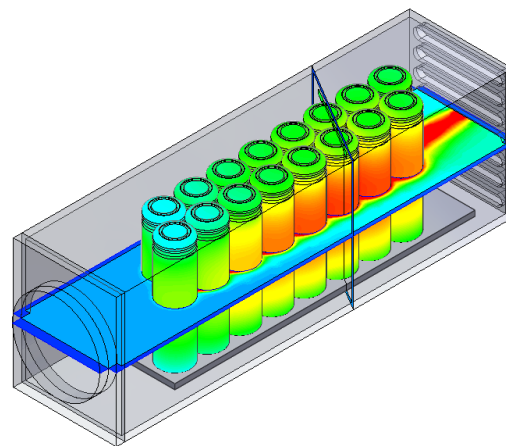


Figure 5. Battery module configuration and sections considered for temperature investigation.

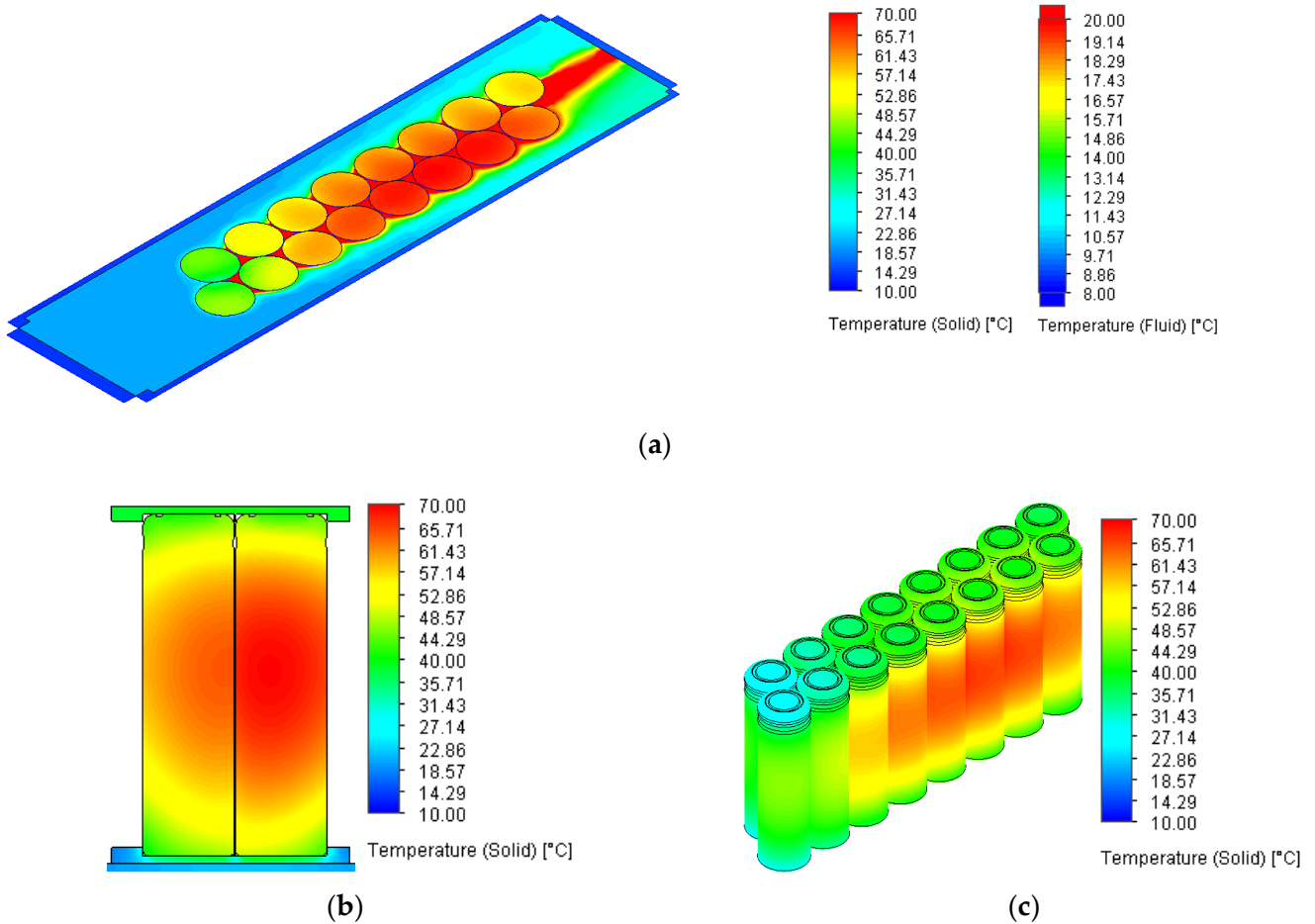


Figure 6. Battery mode thermal behavior for Case #1: (a) air and solid temperature cut plot after 300 s; (b) transversal temperature cut plot through cells after 300 s, in case of direct air cooling; (c) temperature field of the Li-ion cells, in case of air cooling.

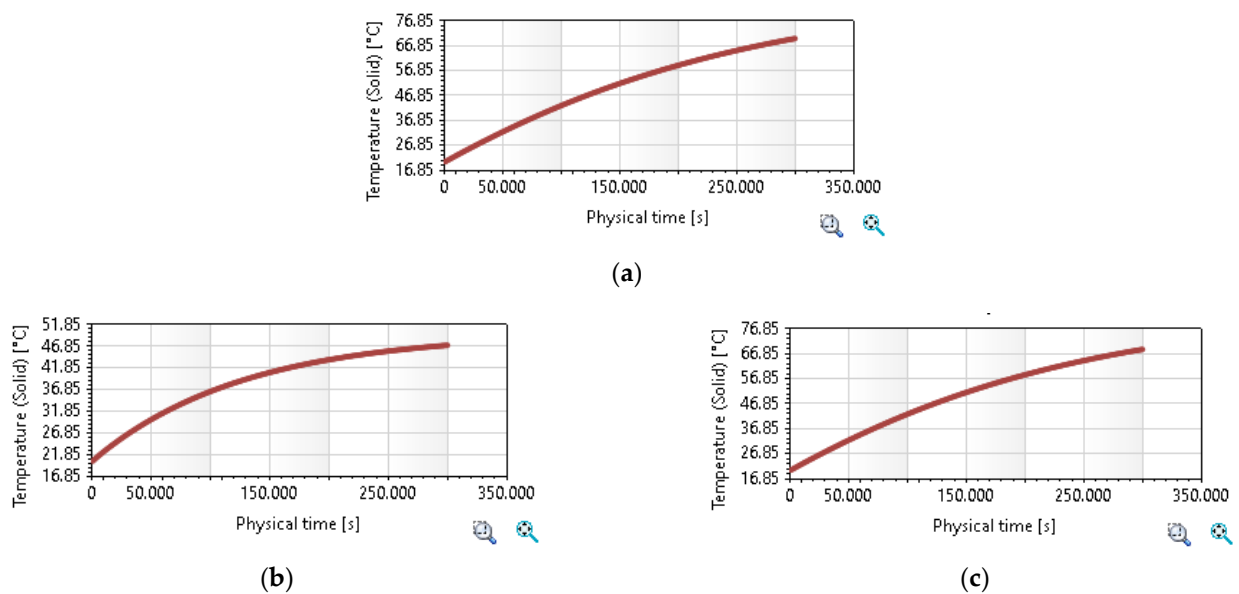


Figure 7. Variation of max temperature regarding: (a) cells in case of air cooling; (b) cell #1 in case of air cooling; (c) cell #5 in case of air cooling.

Case #2—Air Cooling and Use of Flame-Retardant Resin as Heat Transfer Medium

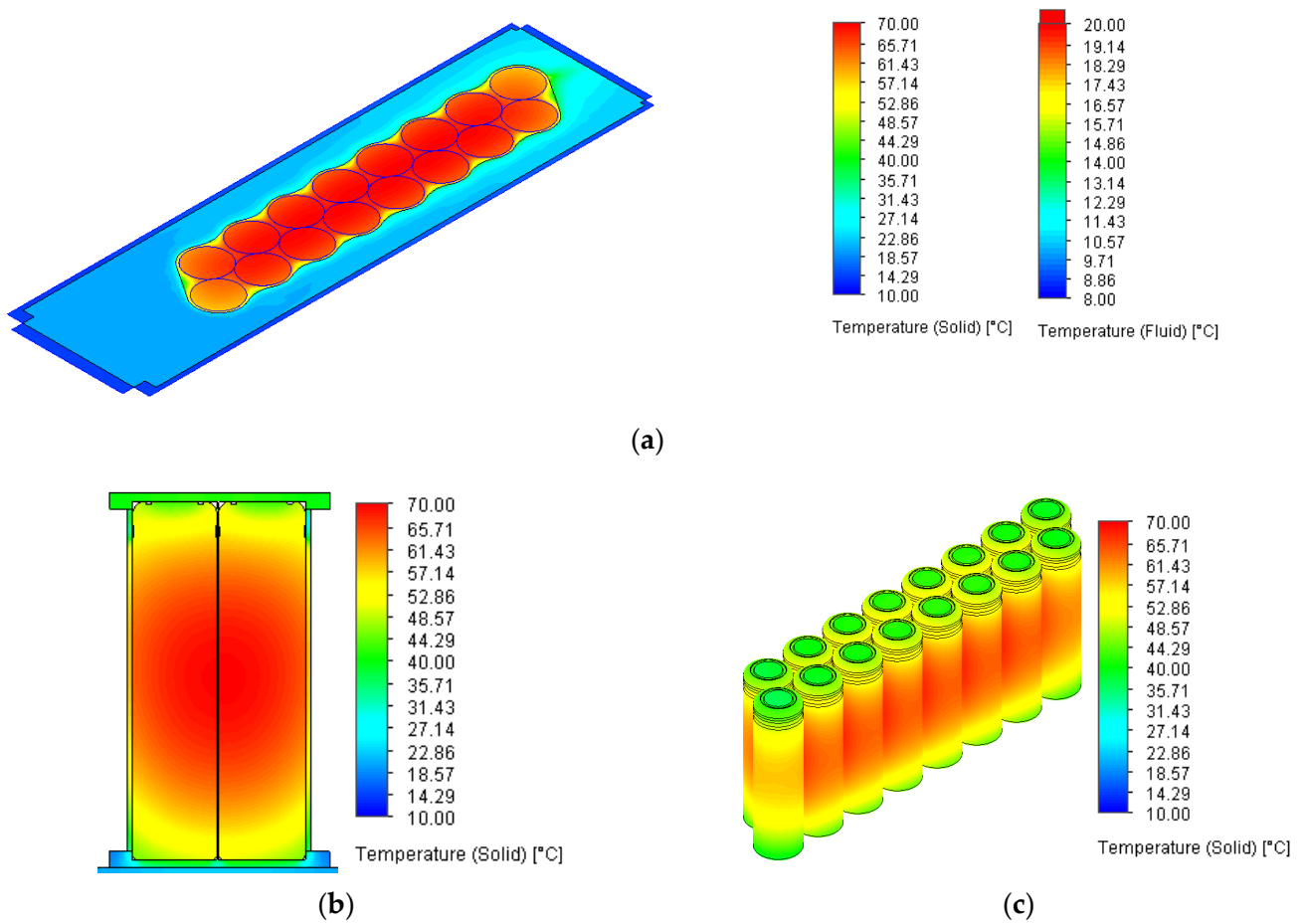


Figure 8. Battery mode thermal behavior for Case #2: (a) air and solid temperature cut plot after 300 s; (b) transversal temperature cut plot through cells after 300 s in case of direct air cooling; (c) temperature field of the Li-ion cells in case of flame-retardant resin used as heat transfer medium.

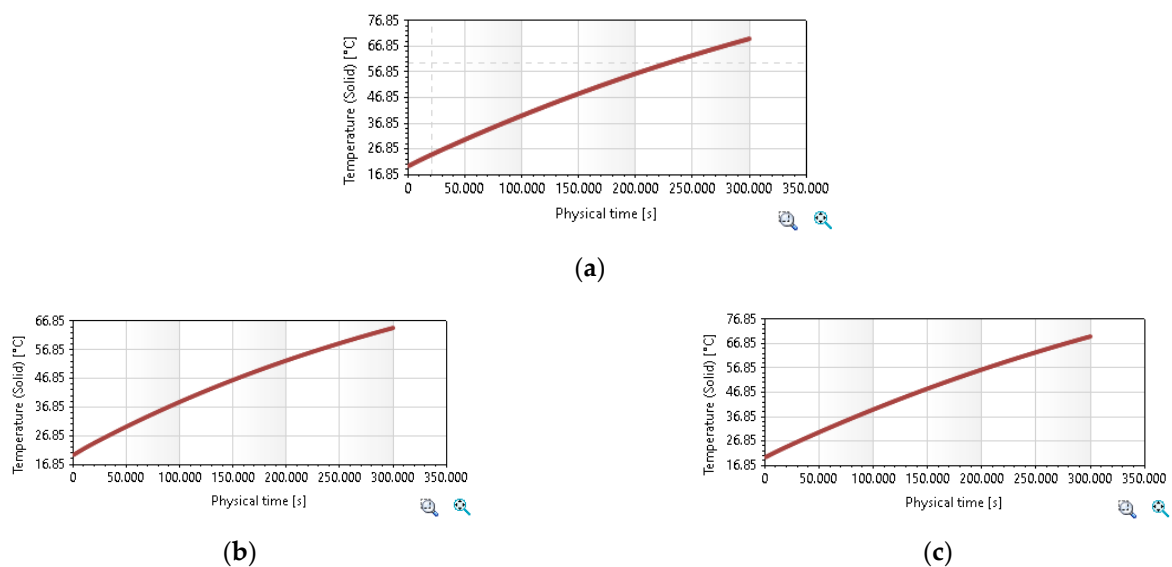


Figure 9. Variation of max temperature regarding: (a) cells in case of flame-retardant resin used as heat transfer medium; (b) cell #1 in case of flame-retardant resin used as heat transfer medium; (c) cell #5 in case of flame-retardant resin used as heat transfer medium.

Case #3—Air Cooling and Use of Composite Resin with Nanomaterials as Heat Transfer Medium

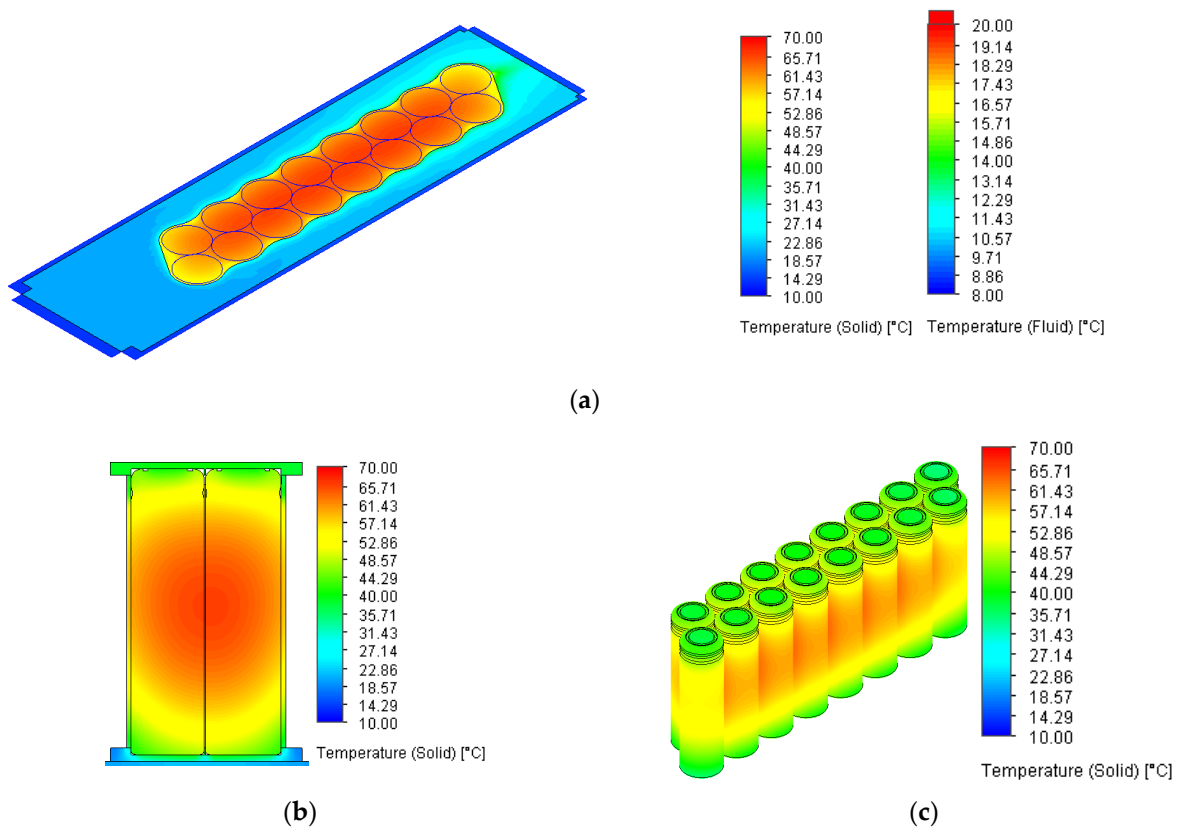


Figure 10. Battery mode thermal behavior for Case #3: (a) air and solid temperature cut plot after 300 s; (b) transversal temperature cut plot through cells after 300 s in case of direct air cooling and use of composite resin with nanomaterials as heat transfer medium; (c) temperature field of the Li-ion cells in case of air cooling and use of composite resin with nanomaterials as heat transfer medium.

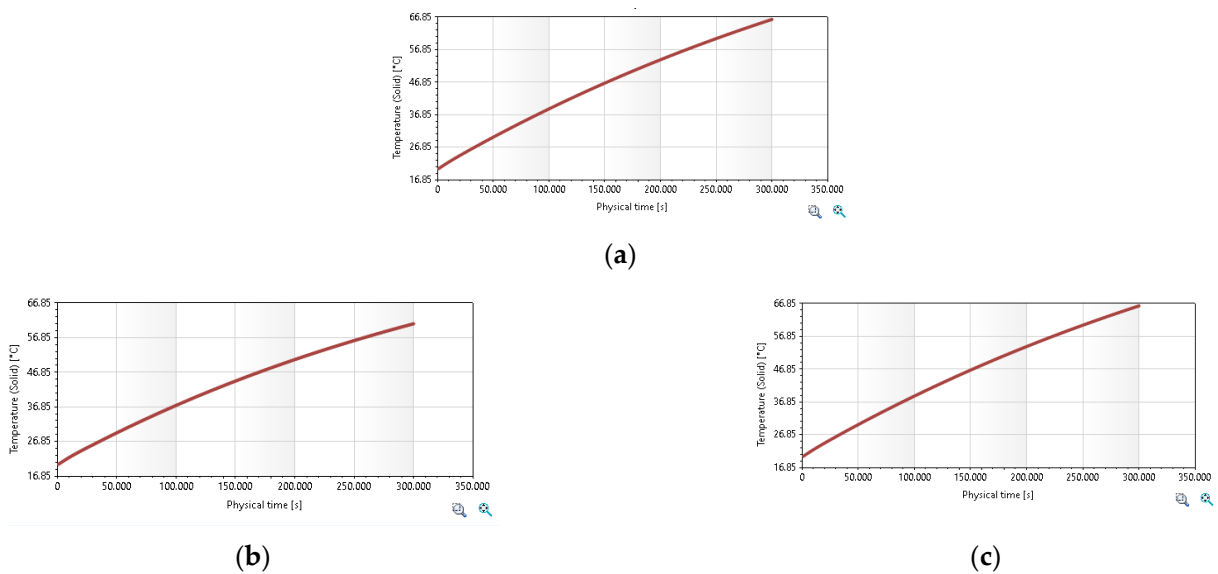


Figure 11. Variation of max temperature regarding: (a) cells in case of air cooling and use of composite resin with nanomaterials as heat transfer medium; (b) cell #1 in case of air cooling and use of composite resin with nanomaterials as heat transfer medium; (c) cell #5 in case of air cooling and use of composite resin with nanomaterials as heat transfer medium.

Case #4—Air Cooling and Use of an Aluminum Block

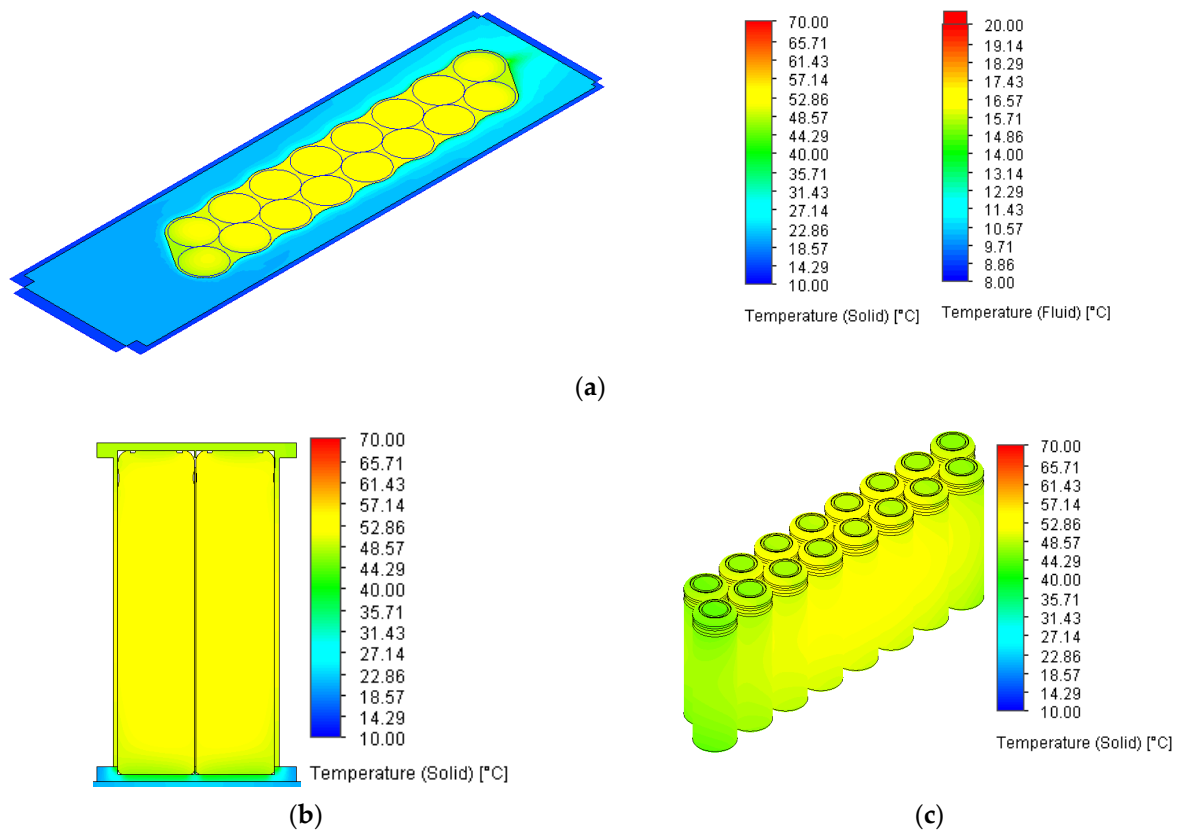


Figure 12. Battery mode thermal behavior for Case #4: (a) air and solid temperature cut plot after 300 s; (b) transversal temperature cut plot through cells after 300 s. in case of direct air cooling and use of an aluminum block; (c) temperature field of the Li-ion cells in case of air cooling and use of an aluminum block.

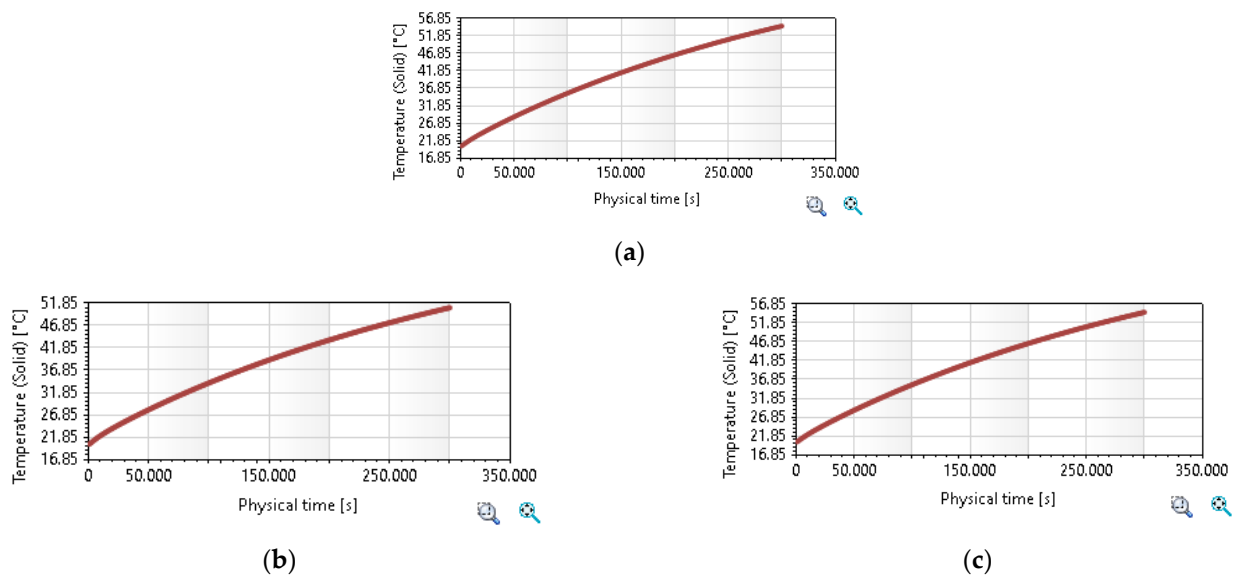


Figure 13. Variation of max temperature regarding: (a) cells in case of air cooling and use of an aluminum block; (b) cell #1 in case of air cooling and use of an aluminum block; (c) cell #5 in case of air cooling and use of an aluminum block.

Case #5—Air Cooling and Use of Flame-Retardant Resin Composite with Nanomaterials and Aluminum Cooling Fins as Heat Transfer Medium

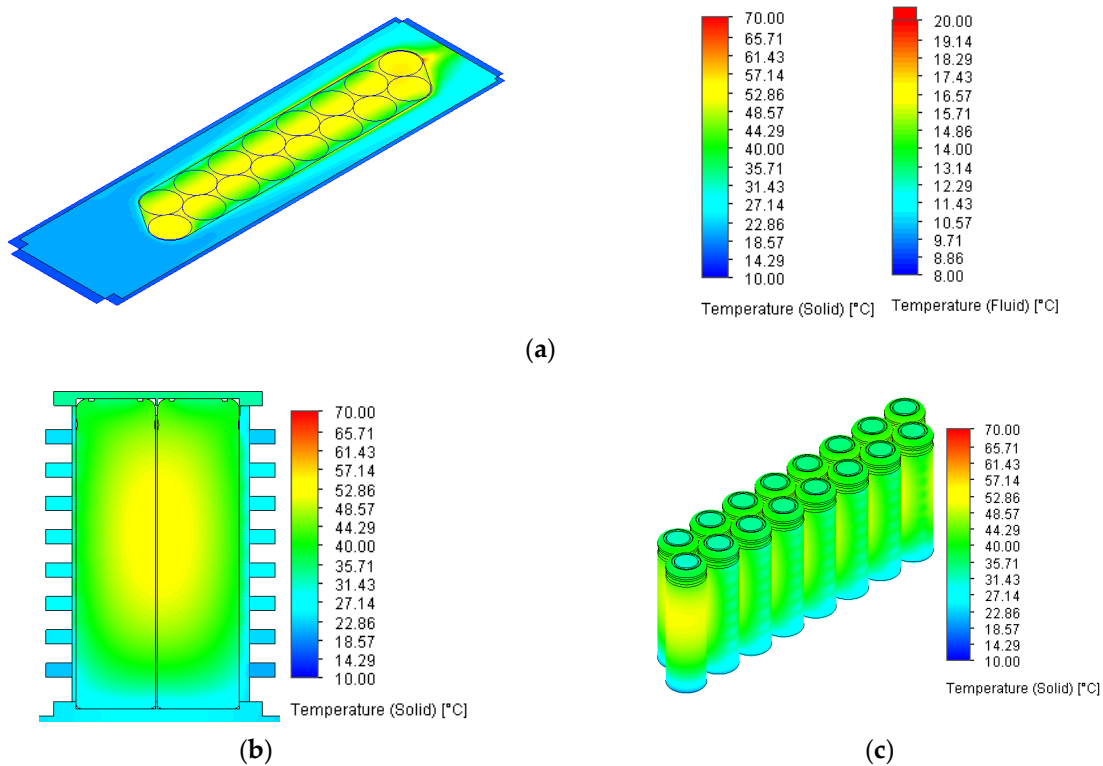


Figure 14. Battery mode thermal behavior for Case #5: (a) air and solid temperature cut plot after 300 s; (b) transversal temperature cut plot through cells after 300 s. in case of direct air cooling and use of flame-retardant resin composite with nanomaterials and aluminum cooling fins as heat transfer medium; (c) temperature field of the Li-ion cells in case of air cooling and use of flame-retardant resin composite with nanomaterials and aluminum cooling fins as heat transfer medium.

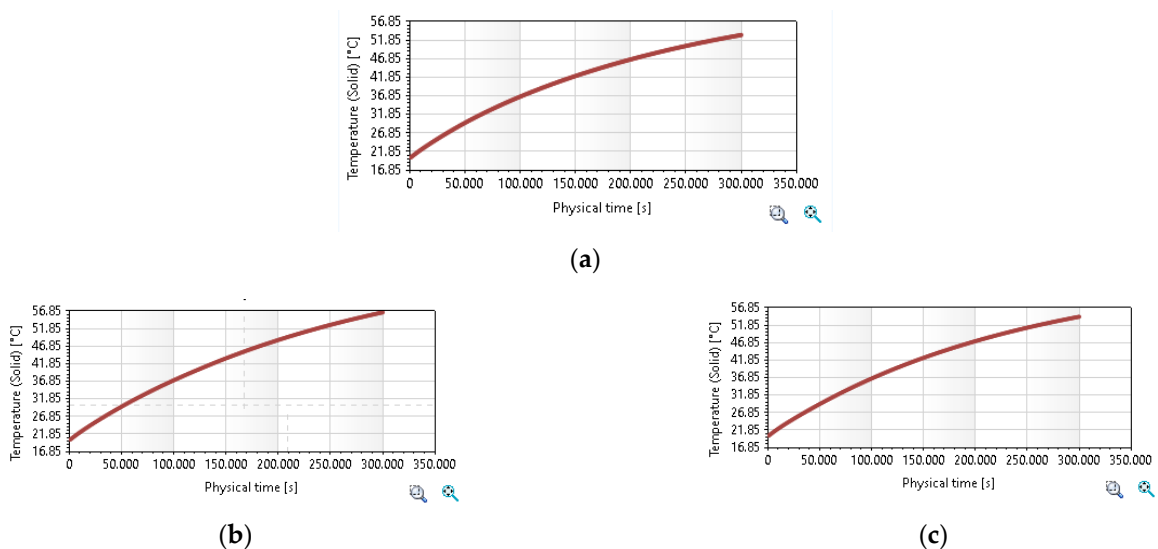


Figure 15. Variation of max temperature regarding: (a) cells in case of air cooling and use of flame-retardant resin composite with nanomaterials and aluminum cooling fins as heat transfer medium; (b) cell #1 in case of air cooling and use of flame-retardant resin composite with nanomaterials and aluminum cooling fins as heat transfer medium; (c) cell #5 in case of air cooling and use of flame-retardant resin composite with nanomaterials and aluminum cooling fins as heat transfer medium.

3.2. Comparative Evaluations of Cell Temperatures

Figure 16 depicts a clustered bar graph that showcases the distribution of battery cells over different temperature ranges for each simulated case. The X-axis depicts temperature ranges in the following intervals: 30...40 °C, 40...50 °C, 50...60 °C, and 60...70 °C.

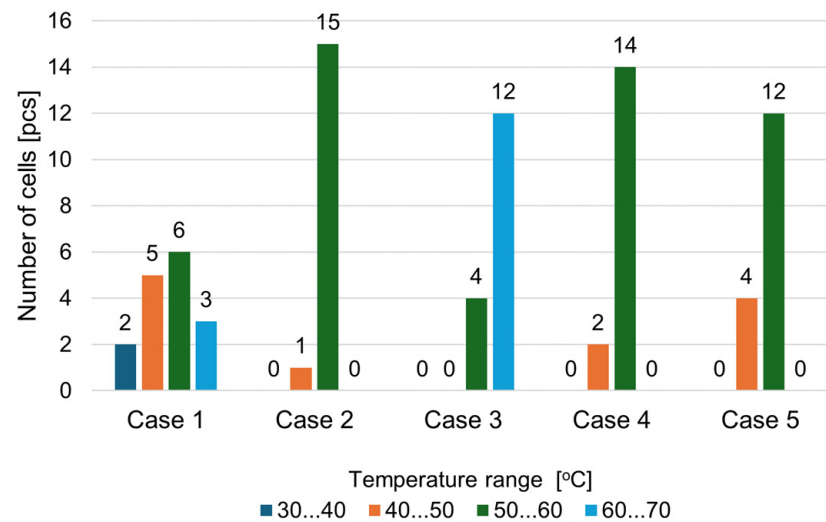


Figure 16. Clustered bar graph of cell distribution on different temperature ranges of the battery module.

The Y-axis displays the quantity of battery cells. By noting the considerable height of the bar, indicating the temperature range of 50–60 °C, in comparison to the other bars, we can deduce that a substantial proportion of battery cells function within this specific temperature range. Comparative evaluations might assist in designing more efficient cooling systems or applying temperature control measures to optimize battery performance and extend its overall lifespan. In addition, researchers can detect potential hot spots or areas of thermal inefficiency inside the battery pack by analyzing the battery cells' temperature distribution.

3.3. Comparative Evaluation of Li-Ion Battery Degradation

From the several methods used to evaluate the degradation of Li-ion batteries, the Arrhenius equation is one of the most commonly used, with implementations in the analysis of power loss [28], capacity loss [29–32], lifetime reduction [33–36], and the generation of thermal runaway phenomena [37]. The Arrhenius equation (Equation (1)) correlates the rate of chemical reactions with temperature, and in this study, it will be used to determine the number of chemical reactions and particularly, the number of degradation processes that occur in the cells for the various proposed battery thermal management cases.

$$k = A \cdot e^{-\frac{E_a}{RT}}, \quad (1)$$

where:

- k [s^{-1}] is the rate constant, which indicates the frequency at which the degradation processes, such as the decomposition of the electrodes' active material or the growth of solid electrolytic interface, occur;
- A ($=3.5 \times 10^{12}$ [s^{-1}]) is the pre-exponential factor, which represents the thermal dependency of the chemical and electrochemical reactions;
- E_a ($=50$ [J/mol]) is the chemical reaction's activation energy, associated with the reaction rate's sensitivity to changes in temperature. It represents the amount of energy needed for activating specific degradation processes at the electrode–electrolyte interface;
- R ($=8.314$ [J/molK]) is the gas constant;
- T [K] is the absolute temperature.

For every simulation time-step, the rate constant calculated for the current temperature was multiplied by the time interval, which finally results in the total number of reactions that occur at the batteries' electrodes during the 300 s, therefore indicating the magnitude of the degradation processes. Using this method, the recorded temperature from every time instance is considered, highlighting the importance of not only maximum temperature, but also of the whole temperature variation curve. The rate constant variation over time, caused by the increase in temperature, for the two mentioned cells in all five proposed cases, is illustrated in Figure 17.

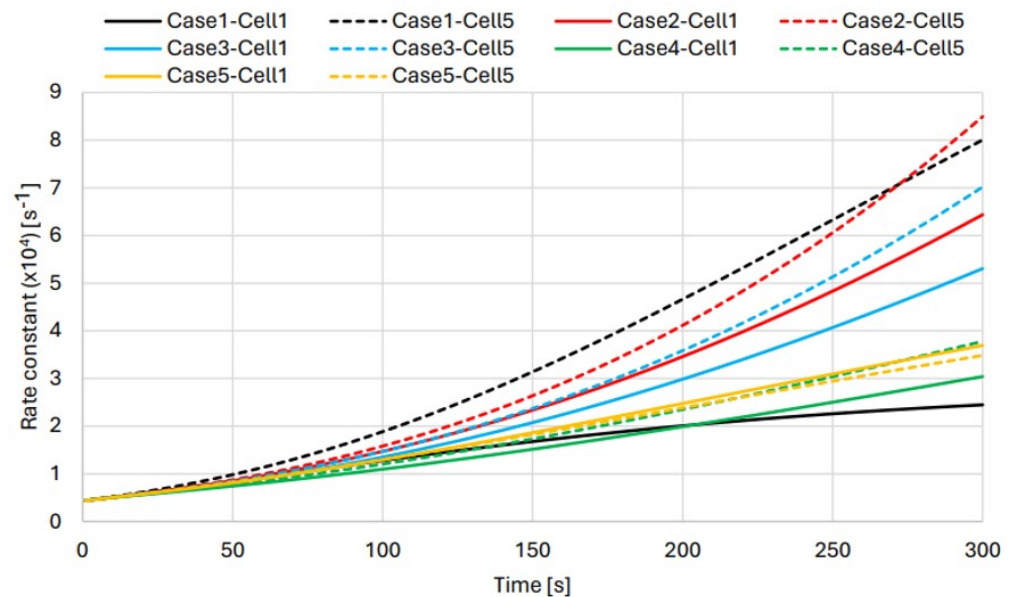


Figure 17. Rate constant variation of cells #1 and #5.

Firstly, the degradation uniformity inside the module is analyzed, which results from the thermal gradients between the cells and impacts the state of health (SoH), not only of the cell with the highest temperature, but also the overall SoH of the entire battery module. Because of the large thermal gradients (over 20 °C at the end of the considered time of 300 s) recorded for the air-cooled solution, the number of degradation processes is higher, with 122% for cell #5 compared to cell #1. This shows that despite having the lowest final temperature at cell #1, the temperature non-uniformity severely impacts the overall SoH of the module, which can lead to electrical imbalances and a lifespan reduction of the entire module. The other solutions, in which the cells are surrounded by a solid material, present significantly better results, from this perspective. For the simple epoxy (Case #2) the difference in degradation is 20.1%, similar to the 20.7% recorded for the nanocomposite (Case #3) and to the 16.9% obtained for the aluminum (Case #4).

The best results in this regard are recorded for the nanocomposite with a heat exchanger (Case #5), with a difference of just 3.1%, proving the importance of heat exchangers in dissipating the excessive heat that is stored in the surrounding material and in creating more uniform temperature distributions.

In the second analysis, a comparison is made regarding the number of chemical reactions and the degradation processes between the cells with the maximum temperature from the five proposed solutions. The comparative results are presented in Figure 18, using heatmap colors for a more suggestive illustration. As previously stated, the air-cooled solution presents the lowest final temperature, but at the same time, the second-highest maximum temperature. Even so, because of the poor heating capacity of air compared to the solid materials used in the other solutions, the temperature variation profile presents a more rapid temperature rise and therefore, a higher number of total chemical reactions that occur during the analyzed 300 s.

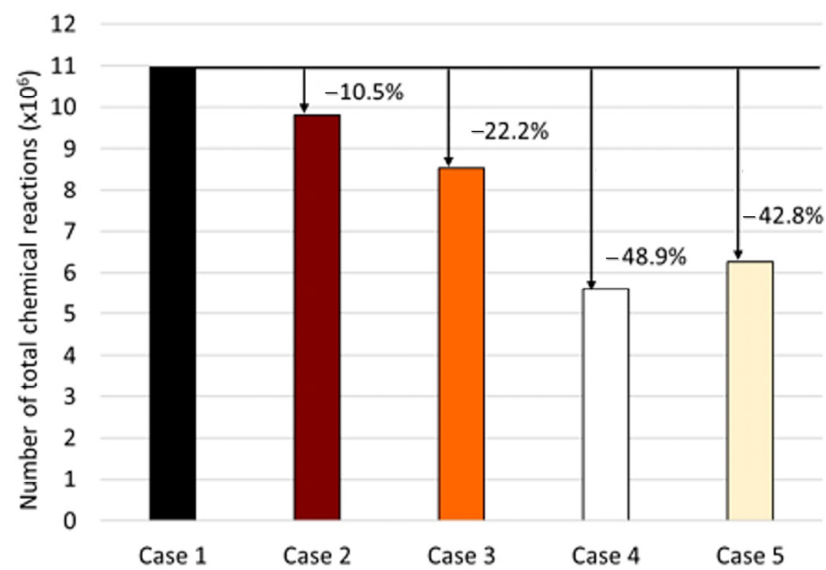


Figure 18. Number of total chemical reactions for cell #5.

In consequence, despite the lower final temperatures, the highest degradation is recorded for the air-cooled solution, which will therefore be used as a reference in the comparison of the other proposed solutions. Despite the previously mentioned higher final temperatures, the epoxy resin solution (Case #2) presents a number of chemical reactions that are 10.5% lower than those of the reference. For Case #3, consisting of the nanocomposite material, the average temperature was 4 °C lower than that of the air-based reference solution, creating a 22.2% lower degradation. Regarding the solution with a heat exchanger (Case #5), although it presents excellent thermal uniformity, as mentioned above, the maximum temperature is 1.8 °C, and the average temperature 1.7 °C higher than that of the solution with the aluminum block (Case #4), leading to a reduction in degradation of 42.8%, while for Case #5, there is a reduction of 48.9% (Figure 18).

It is observed that the constructive solution that continues in the battery module component, i.e., an aluminum block (Case #4), is the best from the point of view of battery life (estimated by the total number of chemical reactions). However, there are limitations in the application of the solution on a large scale in the BTMS construction of batteries due to objective factors such as technological processing difficulties, associated costs, and weight. For this reason and considering that the difference for Case #5 is relatively small (of 6.1%), it can be considered that the solution of using a flame-retardant composite resin, with the addition of nanomaterial and a heat exchanger (aluminum fins), offers the best solution regarding the use of a battery module for the extension of battery life, with the possibility of reducing/eliminating the risk of fire.

Compared to the option of using only resin, without the addition of nanomaterial, the difference in increasing the battery life span using this method can be considered major, with an increase of 20.6%. From the point of view of comparison, only for the cases where the flame-retardant resin is used, it can be stated that the addition of 3 wt.% of nanomaterials led to a significant increase in the battery life span by 11.7%.

4. Conclusions

As a major conclusion regarding this research, it can be stated that thermal gradients are a major point of interest in the design of efficient battery thermal management systems (BTMS), as they greatly impact the overall SoH. Battery modules with low local temperatures but high thermal gradients are a sign of an inefficient allocation of resources, since all the energy consumed for the overcooling of some cells can be considered as wasted. Instead, a more efficient energy distribution would mean the better cooling of the undercooled

cells, avoiding the formation of thermal gradients that lead to electrical imbalance and lifespan reduction.

Adding nanomaterial powders during the preparation of composite materials used in BTMSs can enhance the overall performance, leading to lower average and maximum temperatures, better thermal uniformity, longer lifespan, and a generally better SoH, as well as a potential increase in safety through the use of electrically insulating and fire-resistant materials. The use of heat exchangers proves to be necessary in exploiting the higher thermal performance of composite materials, allowing for a much easier heat dissipation, and leading to excellent thermal uniformity, which is one of the great advantages of surrounding Li-ion battery cells with a thermally conductive material. This leads to a future research directive to optimize the dimensions of the heat exchangers relative to the thickness, shape, and placement of the fins to achieve a (quasi) laminar air flow around the battery module.

Author Contributions: Conceptualization, F.M., I.S. and T.I.C.B.; methodology, F.M.; validation, F.M., I.S. and T.I.C.B.; formal analysis, I.S. and T.I.C.B.; investigation, F.M., I.S. and T.I.C.B.; writing—original draft preparation, F.M., I.S. and T.I.C.B.; writing—review and editing, F.M.; supervision, F.M. All authors have read and agreed to the published version of the manuscript.

Funding: This research received no external funding.

Institutional Review Board Statement: Not applicable.

Informed Consent Statement: Not applicable.

Data Availability Statement: The data presented in this study are available on request from the corresponding author.

Conflicts of Interest: The authors declare no conflicts of interest. The funders had no role in the design of the study; in the collection, analyses, or interpretation of data; in the writing of the manuscript; or in the decision to publish the results.

References

1. Pai, F.-Y.; Shih, Y.-J.; Chuang, Y.-C.; Yeh, T.-M. Supporting Environment Sustainability: Purchasing Intentions Relating to Battery Electric Vehicles in Taiwan. *Sustainability* **2023**, *15*, 16786. [\[CrossRef\]](#)
2. Yang, Z.; Huang, H.; Lin, F. Sustainable Electric Vehicle Batteries for a Sustainable World: Perspectives on Battery Cathodes, Environment, Supply Chain, Manufacturing, Life Cycle, and Policy. *Adv. Energy Mater.* **2022**, *12*, 220038. [\[CrossRef\]](#)
3. Babbitt, C.W. Sustainability perspectives on lithium ion batteries. *Clean Technol. Environ. Policy* **2020**, *22*, 1213–1214. [\[CrossRef\]](#)
4. Yanga, Y.; Okonkwo, E.G.; Huang, G.; Xu, S.; Sun, W.; He, Y. On the sustainability of lithium ion battery industry—A review and perspective. *Energy Storage Mater.* **2021**, *36*, 186–212. [\[CrossRef\]](#)
5. Meshram, P.; Mishra, A.; Sahu, R. Environmental impact of spent lithium ion batteries and green recycling perspectives by organic acids—A review. *Chemosphere* **2020**, *242*, 125291. [\[CrossRef\]](#) [\[PubMed\]](#)
6. Au, H.; Crespo-Ribadeneyra, M.; Titirici, M.M. Beyond Li-ion batteries: Performance, materials diversification, and sustainability. *One Earth* **2022**, *5*, 207–211. [\[CrossRef\]](#)
7. Zanoletti, A.; Carena, E.; Ferrara, C.; Bontempi, E. A Review of Lithium-Ion Battery Recycling: Technologies, Sustainability, and Open Issues. *Batteries* **2024**, *10*, 38. [\[CrossRef\]](#)
8. Liu, C.; Lin, J.; Cao, H.; Zhang, Y.; Sun, Z. Recycling of spent lithium-ion batteries in view of lithium recovery: A critical review. *J. Clean. Prod.* **2019**, *228*, 801–813. [\[CrossRef\]](#)
9. Leng, F.; Tan, C.M.; Pecht, M. Effect of Temperature on the Aging rate of Li Ion Battery Operating above Room Temperature. *Sci. Rep.* **2015**, *5*, 12967. [\[CrossRef\]](#)
10. Xia, H.; Liu, C.; Shen, L.; Yu, J.; Li, B.; Kang, F.; He, Y.-B. Structure and thermal stability of $\text{LiNi}_{0.8}\text{Co}_{0.15}\text{Al}_{0.05}\text{O}_2$ after long cycling at high temperature. *J. Power Sources* **2020**, *450*, 227695. [\[CrossRef\]](#)
11. Waldmann, T.; Wilka, M.; Kasper, M.; Fleischhammer, M.; Wohlfahrt-Mehrens, M. Temperature dependent ageing mechanisms in Lithium-ion batteries—A Post-Mortem study. *J. Power Sources* **2014**, *262*, 129–135. [\[CrossRef\]](#)
12. Lv, S.; Wang, X.; Lu, W.; Zhang, J.; Ni, H. The Influence of Temperature on the Capacity of Lithium Ion Batteries with Different Anodes. *Energies* **2022**, *15*, 60. [\[CrossRef\]](#)
13. Borner, M.; Friesen, A.; Grütze, M.; Stenzel, Y.P.; Brunklaus, G.; Haetge, J.; Nowak, S.; Schappacher, F.M.; Winter, M. Correlation of aging and thermal stability of commercial 18650-type lithium ion batteries. *J. Power Sources* **2017**, *342*, 382–392. [\[CrossRef\]](#)
14. Guan, T.; Sun, S.; Gao, Y.; Du, C.; Zuo, P.; Cui, Y.; Zhang, L.; Yin, G. The effect of elevated temperature on the accelerated aging of $\text{LiCoO}_2/\text{mesocarbon microbeads}$ batteries. *Appl. Energy* **2016**, *177*, 1–10. [\[CrossRef\]](#)

15. Ma, S.; Jiang, M.; Tao, P.; Song, C.; Wu, J.; Wang, J.; Deng, T.; Shang, W. Temperature effect and thermal impact in lithium-ion batteries: A review. *Prog. Nat. Sci. Mater. Int.* **2018**, *28*, 653–666. [[CrossRef](#)]
16. Spitthoff, L.; Shearing, P.R.; Burheim, O.S. Temperature, Ageing and Thermal Management of Lithium-Ion Batteries. *Energies* **2021**, *14*, 1248. [[CrossRef](#)]
17. Siddique, A.R.M.; Mahmud, S.; van Heyst, B. A Comprehensive Review on a Passive (Phase Change Materials) and an Active (Thermoelectric Cooler) Battery Thermal Management System and Their Limitations. *J. Power Sources* **2018**, *401*, 224–237. [[CrossRef](#)]
18. Kim, J.; Oh, J.; Lee, H. Review on Battery Thermal Management System for Electric Vehicles. *Appl. Therm. Eng.* **2019**, *149*, 192–212. [[CrossRef](#)]
19. Zhao, C.; Zhang, B.; Zheng, Y.; Huang, S.; Yan, T.; Liu, X. Hybrid Battery Thermal Management System in Electrical Vehicles: A Review. *Energies* **2020**, *13*, 6257. [[CrossRef](#)]
20. Liu, Z.; Huang, J.; Cao, M.; Jiang, G.; Hu, J.; Chen, Q. Preparation of Binary Thermal Silicone Grease and Its Application in Battery Thermal Management. *Materials* **2020**, *13*, 4763. [[CrossRef](#)]
21. Kang, H.; Kim, H.; An, J.; Choi, S.; Yang, J.; Jeong, H.; Huh, S. Thermal Conductivity Characterization of Thermal Grease Containing Copper Nanopowder. *Materials* **2020**, *13*, 1893. [[CrossRef](#)]
22. Ge, X.; Chen, Y.; Liu, W.; Zhang, G.; Li, X.; Ge, J.; Li, C. Liquid cooling system for battery modules with boron nitride based thermal conductivity silicone grease. *RSC Adv.* **2022**, *12*, 4311–4321. [[CrossRef](#)] [[PubMed](#)]
23. Zhang, Y.; Li, W.; Huang, J.; Cao, M.; Du, G. Expanded Graphite/Paraffin/Silicone Rubber as High Temperature Form-stabilized Phase Change Materials for Thermal Energy Storage and Thermal Interface Materials. *Materials* **2020**, *13*, 894. [[CrossRef](#)] [[PubMed](#)]
24. Jaguemont, J.; Van Mierlo, J. A Comprehensive Review of Future Thermal Management Systems for Battery-Electrified Vehicles. *J. Energy Storage* **2020**, *31*, 101551. [[CrossRef](#)]
25. Buidin, T.I.C.; Mariasiu, F. Parametric Evaluation of Thermal Behavior for Different Li-Ion Battery Chemistries. *Batteries* **2022**, *8*, 291. [[CrossRef](#)]
26. Buidin, T.I.C.; Mariasiu, F. Effects of using fireproof thermal management systems on the lifespan of battery cells. *Case Stud. Therm. Eng.* **2024**, *57*, 104347. [[CrossRef](#)]
27. Dadarlat, D.; Tripon, C.; White, I.R.; Korte, D. Photopyroelectric Spectroscopy and Calorimetry. *J. Appl. Phys.* **2022**, *132*, 191101. [[CrossRef](#)]
28. Liaw, B.Y.; Roth, E.P.; Jungst, R.G.; Nagasubramanian, G.; Case, H.L.; Doughty, D.H. Correlation of Arrhenius Behaviors in Power and Capacity Fades with Cell Impedance and Heat Generation in Cylindrical Lithium-Ion Cells. *J. Power Sources* **2003**, *119–121*, 874–886. [[CrossRef](#)]
29. Käbitz, S.; Gerschler, J.B.; Ecker, M.; Yurdagel, Y.; Emmermacher, B.; André, D.; Mitsch, T.; Sauer, D.U. Cycle and Calendar Life Study of a Graphite | LiNi_{1/3}Mn_{1/3}Co_{1/3}O₂ Li-Ion High Energy System. Part A: Full Cell Characterization. *J. Power Sources* **2013**, *239*, 572–583. [[CrossRef](#)]
30. Tamilselvi, S.; Karuppiyah, N.; Rajagopal Reddy, B. Capacity Fade Modeling of Li-Ion Battery Using Evolutionary Algorithm. *E3S Web Conf.* **2019**, *87*, 1026. [[CrossRef](#)]
31. Zeng, L.; Hu, Y.; Lu, C.; Pan, G.; Li, M. Arrhenius Equation-Based Model to Predict Lithium-Ions Batteries' Performance. *J. Mar. Sci. Eng.* **2022**, *10*, 1553. [[CrossRef](#)]
32. Dvorak, D.; Popp, H.; Bäuml, T.; Simic, D.; Kapeller, H. Arrhenius-Equation Based Approach for Modelling Lithium-Ion Battery Aging Effects. In Proceedings of the ITI Symposium, Dresden, Germany, 4–5 November 2014. [[CrossRef](#)]
33. Kittaneh, O. On the Theory of the Arrhenius-Normal Model with Applications to the Life Distribution of Lithium-Ion Batteries. *Batteries* **2023**, *9*, 55. [[CrossRef](#)]
34. Kim, Y.; Lee, J. Remaining Useful Life Predictions in Lithium-Ion Battery under Composite Condition. In Proceedings of the Annual Conference of the Prognostics and Health Management Society, PHM 2016, Chengdu, China, 19–21 October 2016; pp. 363–369.
35. Kucinskis, G.; Bozorgchenani, M.; Feinauer, M.; Kasper, M.; Wohlfahrt-Mehrens, M.; Waldmann, T. Arrhenius Plots for Li-Ion Battery Ageing as a Function of Temperature, C-Rate, and Ageing State—An Experimental Study. *J. Power Sources* **2022**, *549*, 232129. [[CrossRef](#)]
36. Motapon, S.N.; Lachance, E.; Dessaint, L.A.; Al-Haddad, K. A Generic Cycle Life Model for Lithium-Ion Batteries Based on Fatigue Theory and Equivalent Cycle Counting. *IEEE Open J. Ind. Electron. Soc.* **2020**, *1*, 207–217. [[CrossRef](#)]
37. Jeon, M.; Lee, E.; Park, H.; Yoon, H.; Keel, S. Effect of Thermal Abuse Conditions on Thermal Runaway of NCA 18650 Cylindrical Lithium-Ion Battery. *Batteries* **2022**, *8*, 196. [[CrossRef](#)]

Disclaimer/Publisher's Note: The statements, opinions and data contained in all publications are solely those of the individual author(s) and contributor(s) and not of MDPI and/or the editor(s). MDPI and/or the editor(s) disclaim responsibility for any injury to people or property resulting from any ideas, methods, instructions or products referred to in the content.